Observation of Edge Filamentary Structure Motion during Supersonic Molecular-Beam Injection Using a Fast Camera in Heliotron J

Linge ZANG, Nobuhiro NISHINO[1)], Tohru MIZUUCHI[2)], Shinsuke OHSHIMA[2)], Masaki TAKEUCHI[3)], Keijun KASAJIMA, Mengyu SHA, Kiyofumi MUKAI[4)], Hyunyong LEE, Kazunobu NAGASAKI[2)], Hiroyuki OKADA[2)], Takashi MINAMI[2)], Shinji KOBAYASHI[2)], Satoshi YAMAMOTO[2)], Shigeru KONOSHIMA[2)], Yuji NAKAMURA and Fumimichi SANO[2)]

Graduate School of Energy Science, Kyoto University, Uji, Kyoto 611-0011, Japan
[1)]*Graduate School of Engineering, Hiroshima University, Higashihiroshima 739-8527, Japan*
[2)]*Institute of Advanced Energy, Kyoto University, Gokasho, Uji, Kyoto 611-0011, Japan*
[3)]*Naka Fusion Institute, Japan Atomic Energy Agency, Naka 311-0193, Japan*
[4)]*National Institute for Fusion Science, Toki, Gifu 509-5292, Japan*

(Received 18 October 2012 / Accepted 3 April 2013)

A perpendicular-view fast video camera has been installed in Heliotron J to observe the behavior of filamentary structures of edge plasma turbulence across the last closed flux surface (LCFS). Supersonic molecular-beam injection (SMBI) can greatly increase the edge Hα emission; hence, we used the high imaging rate and shutter speed of the camera to capture the behavior of the fast propagating filamentary structures. A high-pass fast Fourier transform filter on the time dimension was adopted to extract the fluctuation component from the raw data for each pixel. The motion of the filamentary structures was clearly visible when we applied an amplitude threshold to identify the intense structures. In addition, a time-resolved 2D cross-correlation technique was adopted to estimate the poloidal phase velocity of turbulence. The motion direction was found to be reversed dramatically just after an SMBI pulse.

Keywords: filamentary structure, edge fluctuation, edge turbulence, fast camera, SMBI, LCFS, Heliotron J, poloidal velocity

DOI: 10.1585/pfr.8.1402066

1. Introduction

A video camera can provide 2D images of turbulence structures by recording Hα/Dα emissions. The intensity S_α of the Hα/Dα line emission is proportional to the neutral gas density n_0 and also depends on the electron temperature T_e and electron density n_e [1, 2]

$$S_\alpha = n_0 f_3(n_e, T_e) A_{32} \quad (1)$$

where $f_3(n_e, T_e)$ is the ratio of the population density of $n = 3$ to the ground state, which is a nonlinear function of n_e and T_e. In the above equation, A_{32} is the radiative decay time rate of the $n = 3$ to $n = 2$ transition, where n is the principal quantum number. Using gas injection, S_α is greatly enhanced because of the increase of n_0; therefore, the signal-to-noise ratio of the camera image can be high enough to be useful even at a high imaging rate and shutter speed. This is the so-called "gas puff imaging (GPI)" technique [3]. The neutral density of the gas, n_0, provided by the gas puff does not change significantly during the short fluctuation time scale ($\sim$10 μs); hence, the fluctuations in S_α are due to the local evolution of the plasma or propagating plasmoids whose electrons can excite neutral atoms immediately. From the DEGAS2 simulation code and experimental results of Alcator C-Mod, in edge plasmas with $10^{13}\,\mathrm{cm}^{-3} < n_e < 10^{14}\,\mathrm{cm}^{-3}$, D$\alpha$ emission is mainly located in the region $10\,\mathrm{eV} < T_e < 50\,\mathrm{eV}$ [3]. In this temperature range, both n_e and T_e perturbation can cause S_α fluctuation [2]. This interpretation can be somewhat simplified if the electron density and temperature fluctuations are in phase, as expected theoretically and approximately verified using Langmuir probes in DIII-D [4] and TEXT [5]. Although there is still no way to determine whether profile changes during GPI are due to density or temperature changes (or both), turbulence properties such as the coherent structure sizes and velocities are independent of the nonlinearities in $f_3(n_e, T_e)$ and can be evaluated directly from the GPI data [6].

Most of the GPI systems in use [2, 3] have a tangential view, using an inside-vacuum telescope, and observe the plasma structures in the radial–poloidal plane. The camera system used in this study has a perpendicular view. The main differences to the tangential view are that this system

author's e-mail: l-zang@center.iae.kyoto-u.ac.jp

does not contain optical components inside vacuum, and the images are taken on the poloidal–toroidal plane.

SMBI is well known as a directional gas fueling method [7–10]. It is demonstrated to be not only an effective fueling method but also an effective edge modification technique for fusion devices [8]. Meanwhile, the high Hα emission during SMBI provides an advantage for using a fast camera. In this paper, we describe the application of a fast video camera to observe the filamentary structures near LCFS in an SMBI-fueled plasma.

2. Equipment Setup

Heliotron J is a medium-sized, helical-axis heliotron device ($\langle R_0\rangle/\langle a\rangle = 1.2\,\mathrm{m}/0.17\,\mathrm{m}$, $\langle B_0\rangle \leq 1.5\,\mathrm{T}$) with an $L = 1/M = 4$ helical coil [11, 12]. As shown in Fig. 1, a NAC fx-k5 fast video camera has been setup at a horizontal perpendicular-view window at #11.5 port [13, 14]. The optical path of the camera system and the observation region of the plasma are illustrated in Fig. 2 (a). The optical axis of the object lens is perpendicular to the torus. The object plane of the object lens was adjusted to be close to LCFS. An SMBI nozzle was also installed at the same port for fueling control, with the gas beam parallel to the optical axis of the object lens. Therefore, the camera signal is obtained mainly from near the outer LCFS where the gas beam is injected. A typical raw image during SMBI is shown in Fig. 2 (b), which shows a bright spot around the beam-crossing area near LCFS. In this image, the horizontal direction indicates the toroidal direction of the torus (also the X direction in this paper) and the vertical direction indicates the poloidal direction (also the Y direction in this paper). The emission enhancement by SMBI allows the camera to be used at a frame rate of up to 168,000 fps with 32×48 pixels and a 5 μs shutter speed.

To estimate the actual pixel size, information about the radial position of the Hα emission region was required. In this experiment, we used the approximate position of LCFS as the emission region, which is 41.66 cm from the object lens, as illustrated in Fig. 2 (a). In other devices, such as the Alcator C-Mod, the GPI signal is mainly ob-

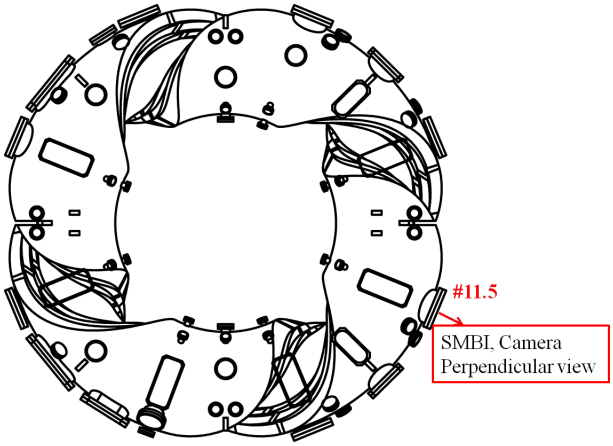

Fig. 1 Top view of Heliotron J showing the toroidal positions of #11.5 SMBI and the fast camera.

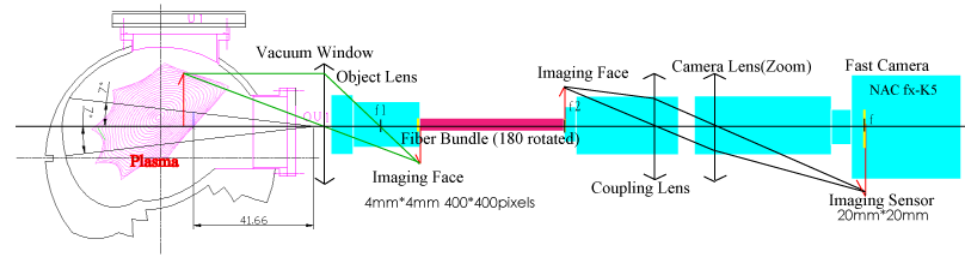

(a)

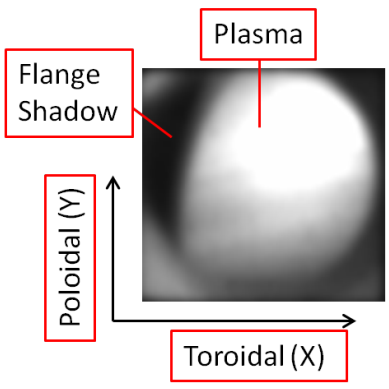

(b)

Fig. 2 (a) Optical path of the fast camera at #11.5; (b) raw image from the #11.5 camera during SMBI (at 80,000 fps).

tained from near the separatrix. The center of the GPI emission cloud is 5 mm outside the separatrix, where $T_e \sim 25$ eV. The radial thickness of the emission cloud is 2 - 3 cm [1]. The error from the radial position estimation is small. For example, a 2 cm error in the radial position will only induce a 2/41.66 ~ 5% error in pixel size. From the optical path in Fig. 2 (a), we estimated the actual pixel size to be about 1.6 mm, which in turn yielded an image area of 51.8 mm × 77.8 mm.

3. Data Analysis and Results

Turbulence structures are observed as being "frozen" in a single image, with the shutter opening duration (~5 μs) shorter than the typical fluctuation time scale (~10 μs). Therefore, structure features such as size and stretch direction could be extracted from the images. If the framing rate of the camera is faster than the lifetime of the turbulent structures within the field of view, the turbulence motion can be followed and continuous images can be correlated to infer the motion velocity of turbulence. In this section, we will focus on the analysis techniques used to capture the behavior of the filamentary structures.

3.1 Extraction of filamentary structures

In this subsection, an example video taken of an SMBI discharge at 168,000 fps and a frame size of 51.8 mm × 77.8 mm will be analyzed. For this discharge, the magnetic configuration was the standard one for Heliotron J and the opening duration of the SMB nozzle was 100 μs. Some of the main plasma parameters in this discharge are given in Fig. 3. The sharp increase in the Hα signal (#11.5Hα), which is measured at the same toroidal section as SMBI, clearly shows the arrival timing (~243 ms) of the molecular beam. Both plasma density and stored energy increased after SMBI. A detailed discussion on the SMBI fueling control in Heliotron J is described in [10].

One of the raw images from this video is shown in Fig. 4 (a). From this perpendicular view, the pixel signal I_{raw} is mainly obtained from the line-integrated emission across the depth of field (DOF) around LCFS, where the Hα emission is supposed to be intense. Moreover, I_{raw} contains both a long-time-scale component, "background" I_{bg}, from across DOF, mainly attributed to the increase and decrease in n_0, and a short-time-scale fluctuation components, $\tilde{I}$, from the turbulent plasma structures [15]. Therefore, pre-processing was applied to make the filament structures more visible by removing the "background" and highlight the fluctuation components. A high-pass fast Fourier transform (FFT) filter was applied to obtain the fast component of fluctuation $\tilde{I}$. The cut-off frequency was set to 10 kHz in this study, which removed most of the slow components brought about by the variation in gas pressure. The "background" component is calculated as $I_{bg} = I_{raw} - \tilde{I}$. To relate the camera signal with the density fluctuation, the normalized fluctuation $\tilde{I}/I_{bg}$ is

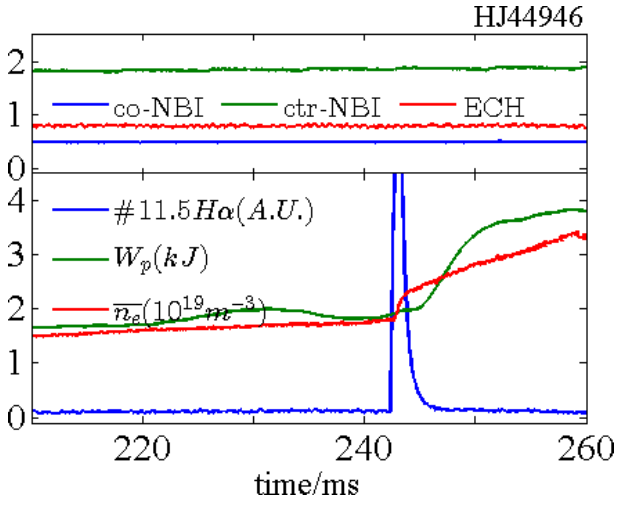

Fig. 3 Plasma parameters for Shot No. 44946, where n_e is the linear-average electron density, Wp is the diamagnetic energy, #11.5 Hα is the signal from the Hα ray detector at the #11.5 section.

used. If the fluctuation in T_e is smaller than and/or in phase with n_e, the image of $\tilde{I}/I_{bg}$ is approximately proportional to the normalized density fluctuation $\widetilde{n_e}$. (It has to be noted that $\tilde{I}/I_{bg}$ is neither equal nor exactly proportional to $\widetilde{n_e}$, since $\tilde{I}$ is the line integration of the emission across the relatively small-sized turbulence structure, while I_{bg} is the line integration of the emission across the whole Hα emission region.) The curves of I_{raw}, $\tilde{I}$, I_{bg}, and $\tilde{I}/I_{bg}$ are shown in Fig. 5. Figures 4 (b) and (c) show the images of $\tilde{I}$ and I_{bg}, respectively. In Fig. 4 (b), we can clearly recognize both positive (white) and negative (black) filamentary patterns of fluctuation. In Fig. 4 (c), the upper part of the background image is much brighter than the lower part because the former is around the gas injection spot, closer to the nozzle and lens.

The fluctuation data in Fig. 4 (b) is filtered with an amplitude threshold to extract the more intense density fluctuation structures [16]. In this paper, the amplitude threshold for each point is set to 1σ, where σ(X, Y) is the normalized standard deviation (STD) of $\tilde{I}/I_{bg}$ at a pixel point (X, Y) during the sliding time window of 100 μs. The blue line in Fig. 4 (e) shows $\tilde{I}/I_{bg}$ along a poloidal line at X = 16 illustrated in Fig. 4 (a). The positive threshold (red line) indicates the density-peaking structures, such as a "blob" or the crest of an intense wave. The negative threshold (black line) indicates the density-hollow structures like a "hole" or the trough of an intense wave. We can identify a density-hollow structure, as illustrated in region (1), and a peaking structure, as illustrated in (2). If we define the width of the shadowed region in the figure as that of the structure, the hollow structure is ~12 mm wide and the peaking structure is ~17 mm wide. Figure 4 (d) is updated from Fig. 4 (b) using the amplitude threshold, where the white color indicates a fluctuation larger than σ, black indicates a fluctua-

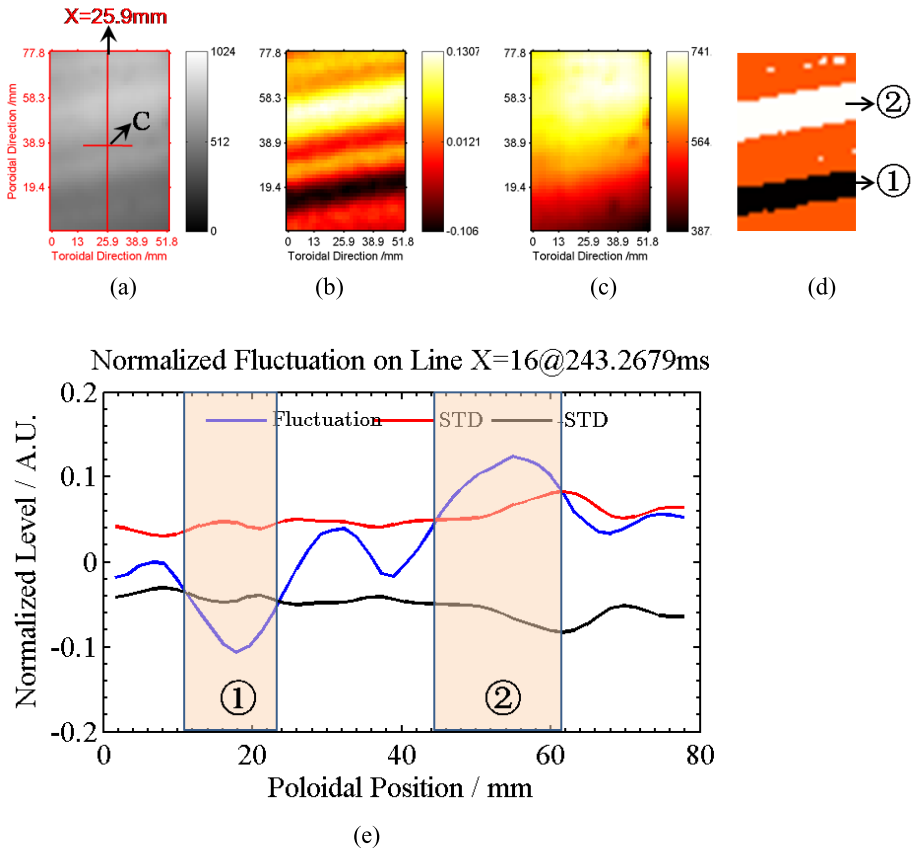

Fig. 4 Images from shot No. 44946. The imaging speed is 168,000 fps. (a) A raw image. Positions of mid-line x = 25.9 mm and center point C (25.9 mm, 38.9 mm) are labeled. The directions of the X-axis and Y-axis are the same as shown in Fig. 2 (b). (b) A normalized fluctuation ($\tilde{I}/I_{\rm bg}$) image. (c) A background image. (d) An updated image with amplitude threshold. (e) The normalized fluctuation signal along the mid-line (blue), positive (red), and negative (black) standard deviation during the time window. Negative and positive fluctuation regions (1) and (2) correspond to the density peak structure and hollow structure in (d), respectively.

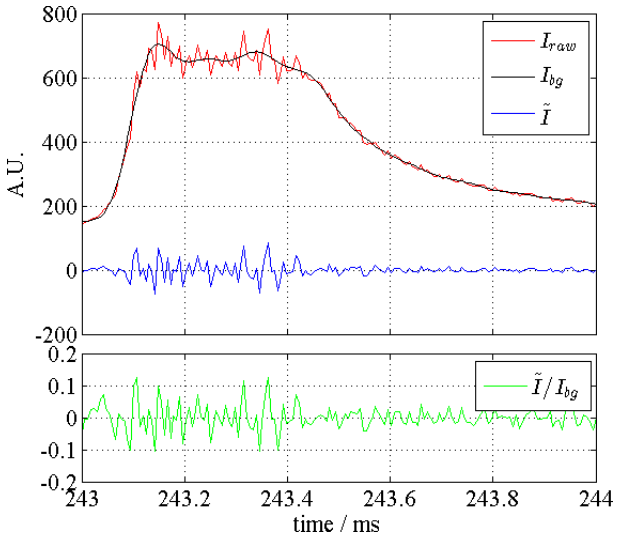

Fig. 5 Data at point C. Red line indicates the camera's raw signal. Blue line indicates the filtered-out fluctuation signal. Black line indicates the background signal. Green line indicates the normalized fluctuation signal of the background.

tion less than $-\sigma$, and red indicates a fluctuation between $-\sigma$ and σ.

3.2 Poloidal velocity estimation

Some continuous images of filamentary structures recorded during SMBI in shot No. 44946 are shown in Figs. 6 (a)–(d). In these figures, upward is in the electron diamagnetic direction (De). From these images, the velocity can be readily estimated. Taking Fig. 6 (a) as an example, five continuous frames (243.089 - 243.119 ms) recorded just after the SMB's arrival are shown. The filament indicated by the arrow travelled approximately 48 pixels in the poloidal direction during this time span. Considering the real size per pixel, ~1.6 mm, we calculated the poloidal velocity, $v_{\theta f} = 48 \times 1.6/(243.119 - 243.089) = 2.5 \times 10^3$ m/s. The propagating direction is downward, which is the ion diamagnetic direction (Di). In these images, it is interesting to note that, during the time span in which $I_{\rm raw}$ is still enhanced by SMBI, the filamentary structure's velocity changes to the De direction, as shown in Fig. 6 (b). After SMBI, in Figs. 6 (c) and (d), the structure's motion returns to the Di direction, and the velocity

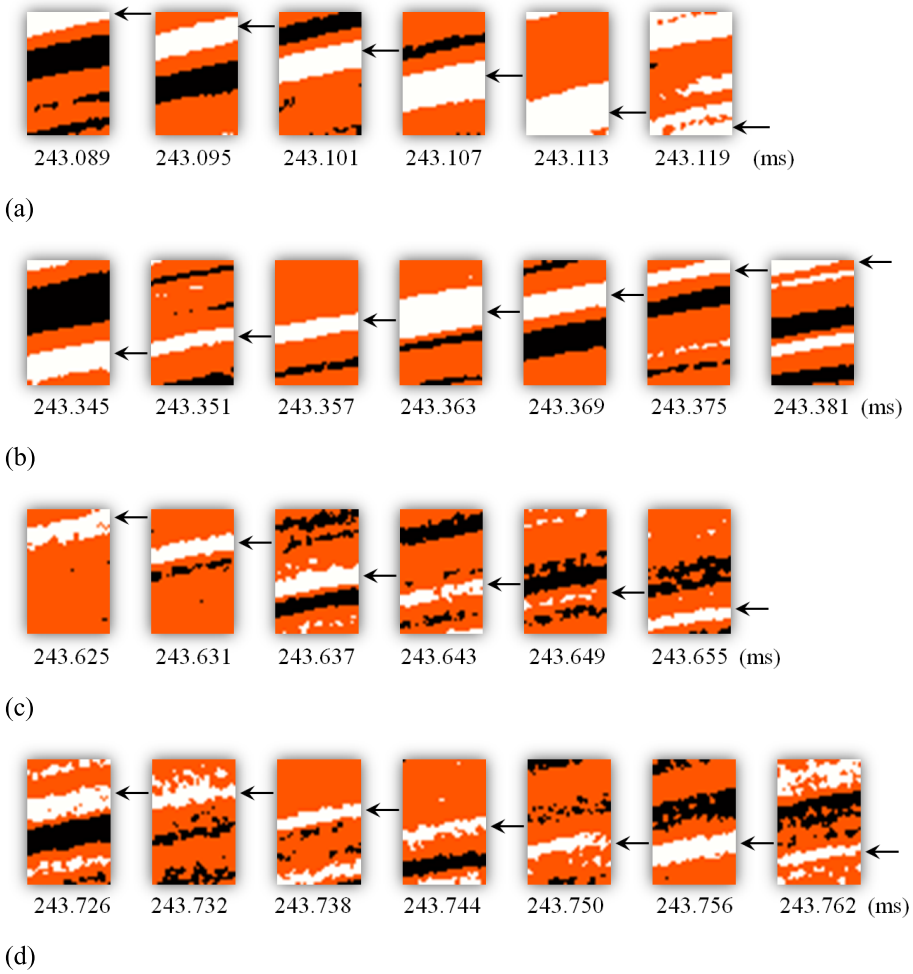

Fig. 6 Updated images from shot No. 44946. (a) 243.089 - 243.119 ms, ~2.5 km/s to Di; (b) 243.345 - 243.381 ms, ~2 km/s to De; (c) 243.625 - 243.655 ms, ~2 km/s to Di; (d) 243.726 - 243.762 ms, ~1 km/s to Di; Upward is the De direction.

slows down to about 1 km/s.

This method of calculation by direct observation is reliable when there is a clear structure crossing the window. However, because the field of view is very narrow, it is not easy to entirely catch the motion of a structure. Another method is to use a cross-correlation technique to estimate the phase velocity of turbulence. The details of a time-resolved 2D cross-correlation technique for GPI data are described in ref. [17]. In shot No. 44946, we used a time window of ±5 frames, which is $10 \times 6\,\mu s = 60\,\mu s$, to examine the cross-correlation between the pixel data of one frame and the following frame. The lag of the cross-correlation is set from −11 to +11 pixels, corresponding to an actual velocity of −4.1 - 4.1 km/s. The calculated region is limited to 19.4 mm < Y < 58.3 mm along the poloidal line at X = 25.9 mm in Fig. 4 (a). Figure 7 is the calculated poloidal velocity, where the error bars indicate standard deviation and the positive direction indicates De direction. During the period 243.0 - 243.2 ms, the velocity is in the Di direction. Then, from 243.2 to 243.6 ms, the velocity reversed to the De direction and dropped from about 2 km/s to zero. Just after 243.6 ms, the motion direction reversed

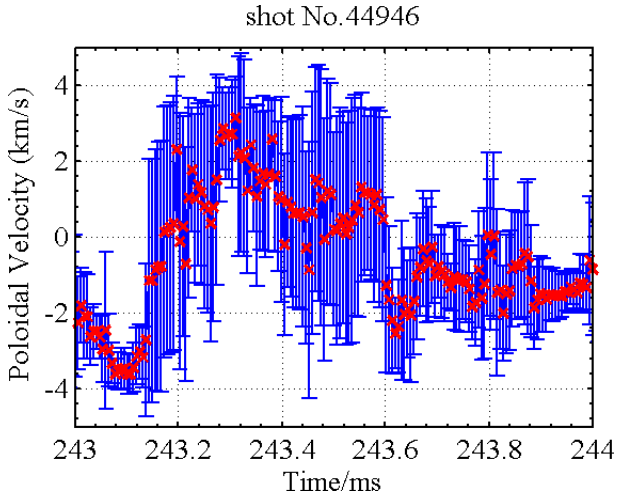

Fig. 7 Poloidal velocity during SMBI. The error bar is from the standard deviation of the results along the specified poloidal line, and the positive direction indicates the De direction.

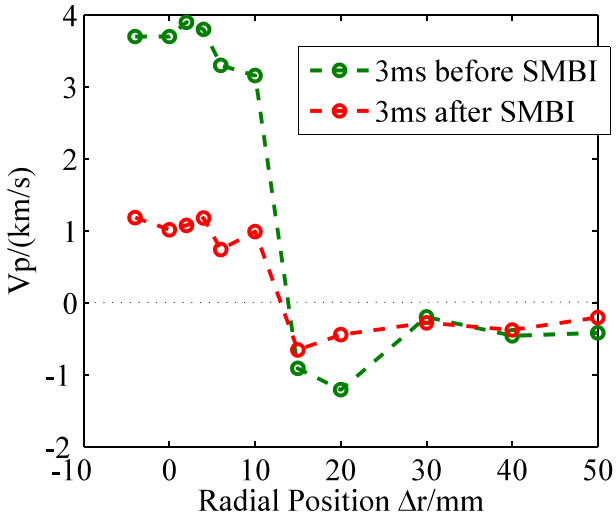

Fig. 8 Turbulence phase velocity in the poloidal direction at #14.5 in Heliotron J, measured by Langmuir probe array. Green line indicates 3 ms before SMBI, and red line indicates 3 ms after SMBI. The positive direction indicates the De direction.

again to the Di direction, and the velocity value varied from 2 km/s to about 1 km/s. All velocity values estimated from Fig. 6 show quite good coincidence with the results shown in Fig. 7.

4. Discussion

The $E \times B$ velocity shear layer (VSL) near the edge has been found in many magnetically confined fusion devices. The Langmuir probe measurement at #14.5 section of Heliotron J reveals a clear VSL, as illustrated in Fig. 8. VSL is located between $\Delta r = 10$ and 15 mm, and does not move before or after SMBI. The turbulence motion inside VSL is in the De direction, and that outside VSL is in the Di direction.

Although the reason for the direction reversal mentioned in Sec. 3.2 is unknown at present, one speculation is that the main Hα emission region shifts inward across VSL because of the strong cooling effect and/or the gas penetration by SMBI. The DOF of the object lens has a certain thickness; therefore, even if the emission region is shifting, it can still be in the DOF and provide a clear image on the camera sensor. This means we must be very careful with the perpendicular-view data, and try to get some radial position information of the main emission region. For this reason, combining these data with Langmuir probe data is a possible solution to this problem, which will be investigated in the future.

Note that at the SMBI arrival-timing window of 243.0 - 243.2 ms, the velocity estimated in both Figs. 6 (a) and 7 might be affected by the fast expansion of the gas cloud. The background emission I_{bg} in Fig. 5, which is proportional to the fluctuation in the neutral gas density $\widetilde{n_0}$, increased quickly during this period. If $\widetilde{n_0}$ varied quickly enough compared to the filter, the $\tilde{I}$ signal we extracted may also be affected. However, after 243.2 ms, I_{bg} varies slowly, which means the component of $\widetilde{n_0}$ will be removed from $\tilde{I}$ by the high-pass filter.

5. Summary

In this paper, we reported on the edge filamentary structures observed by a perpendicular-view camera and the analysis methods used to make the results more visible. The spatial filamentary structure was extracted using a high-pass FFT filter in the time dimension. A threshold amplitude was then employed to extract intense filamentary structures. Using these images, we could directly estimate the poloidal velocity of these structures. A time-resolved 2D cross-correlation technique was also applied to estimate the structure's velocity. The results from the two methods roughly agreed. During an SMBI discharge, it was observed that the poloidal velocity of the filamentary structures reversed during the SMB injection. One possible reason for this is that the intense emission region shifted inward because of the injected gas. Therefore, further work is needed to identify the main emission region using a Langmuir probe.

Acknowledgments

The authors are grateful to the Heliotron J technical staff for conducting the experiments. We also thank Dr. Shinichiro KADO for fruitfull discussions. This work was performed with the support and under the auspices of the NIFS Collaborative Research Program and JSPS Asian CORE Program.

[1] S.J. Zweben and D.P. Stotler *et al.*, Phys. Plasmas **9**, 1981 (2002).
[2] D.P. Stotler *et al.*, J. Nucl. Mater. **313-316**, 1066 (2003).
[3] S.J. Zweben *et al.*, Nucl Fusion **44**, 134 (2004).
[4] D.L. Rudakov *et al.*, Plasma Phys. Control. Fusion **44**, 717 (2002).
[5] M.A. Meier *et al.*, Phys. Rev. Lett. **87**, 500 (2001).
[6] S.J. Zweben *et al.*, Phys. Plasmas **17**, 102502 (2010).
[7] L. Yao, *New Developments in Nuclear Fusion Research* (Nova Science Publishers, 2006) pp.61-87.
[8] L. Yao and J. Baldzuhn, Plasma Sci. Technol. **5**, 1933 (2003).
[9] T. Mizuuchi *et al.*, Contrib. Plasma Phys. **50**, 639 (2010).
[10] T. Mizuuchi *et al.*, J. Nucl. Mater. **415**, S443 (2011).
[11] F. Sano *et al.*, J. Plasma Fusion Res. Series **3**, 26 (2000).
[12] T. Obiki *et al.*, Nucl. Fusion **41**, 833 (2011).
[13] N. Nishino *et al.*, J. Nucl. Mater. **363–365**, 628 (2007).
[14] L. Zang *et al.*, Plasma Sci. Technol. **15**, 213 (2013).
[15] B.D. Dudson *et al.*, Plasma Phys. Control. Fusion **50**, 124012 (2008).
[16] T. Windisch *et al.*, PPPL Reports 4371 (2008).
[17] S.J. Zweben *et al.*, Plasma Phys. Control. Fusion **54**, 025008 (2012).